Sparse Deconvolution of Proton Radiography Data to Estimate Water Equivalent Thickness Maps

Sylvain Deffet,[1] Paolo Farace,[2] and Benoît Macq[1, a)]

[1)] *Institute of Information and Communication Technologies, Université catholique de Louvain, Louvain-La-Neuve, 1348, Belgium*

[2)] *Proton Therapy Unit, Hospital of Trento, Trento, 38100, Italy*

(Dated: March 4, 2020)

Purpose: In proton therapy, the conversion of the planning CT into proton stopping power is tainted by uncertainties which may jeopardize dose conformity. Proton radiography provides a direct information on the energy reduction of protons in the patient. However, it is currently limited by the degradation ('blurring') of the 1-D depth-dose deposition profiles which constitutes the pixels.

Methods: An iterative algorithm is implemented to extract high resolution water equivalent thickness (WET) maps from the measurements of depth-dose profiles. The method relies on the assumption that those curves are a function of the WET, which can benefit from a sparse representation.

Results: When used without relying on any prior knowledge derived from the planning CT, the method already outperforms the published one in terms of accuracy. We also propose a variant which integrates the planning CT in a robust fashion to further improve the deconvolution result and reach a submillimeter accuracy on the estimated WET. The methods are applied to both synthetic data and actual proton radiography acquisitions on phantoms.

Conclusion: Besides the increase in accuracy achieved in the estimation of WET maps from proton radiography data, we demonstrate that the proposed deconvolution algorithm is also more robust with respect to confounding factors such as residual set-up errors or changes in the anatomy. Therefore, proton radiography using a range probe provides both the required accuracy to assess and reduce range uncertainty in proton therapy and the simplicity of integrated-mode proton radiography.

Keywords: Proton Radiography, Particle Imaging, Range Uncertainty, Multi Layer Ionization Chamber, Deconvolution.

[a)]Electronic mail: benoit.macq@uclouvain.be

I. INTRODUCTION

Proton therapy has the potential to confine most of the dose to the target thanks to the physical property of protons called the Bragg peak. Unlike photons used in conventional radiation therapy, protons deliver a sharp dose at a precise location which depends on their entrance energy and their interactions with the molecules on their way. However, a consequence of this dosimetric property is that the range of the protons inside the patient must be accurately predicted to ensure conformity between the prescribed dose and the delivered one. In clinical practices, proton ranges are predicted based on a planning CT of which the Hounsfiels Units (HU) are commonly converted to proton energy loss rates, also called proton stopping powers, via a piecewise linear relationship[1]. Unfortunately, this process is tainted by uncertainties to which others add up during treatment planning and delivery. To take them into account in the planning phase, treatment margins of 3.5% are conventionally used, *de facto* jeopardizing dose conformity[2].

During the last decade, a variety of approaches have been investigated to improve the prediction of the Bragg peak position and reduce the treatment margins such as prompt-gamma imaging, dual energy CT, PET, iono-acoustic, and proton imaging[3]. In the latter, a detector placed after the patient provides a direct measurement of the decrease in proton energy. In conjunction with x-ray based planning imaging, proton range data could be used to validate and even improve the process of converting the HUs of the planning CT into stopping powers[4–8].

Two main types of proton radiography systems are investigated worlwide. On the one hand, list-mode proton radiography tracks protons individually[9]. Both their energy loss and their trajectories are measured, which requires complex hardware to be placed before and after the patient. On the other hand, the integrated mode proton radiography integrates the contribution of every proton during the irradiation time of a pencil beam shot. If this approach implies only moderate requirements in terms of data acquisition rates and hardware capabilities, it comes at the cost of signal degradations resulting from the presence of lateral inhomogeneties along the path of the beam and, to a lesser extent, from multiple Coulomb scattering (MCS).

Among the integrated mode proton radiography techniques, the use of multilayer ionization chambers (MLIC) has benefited from a recent body of research which demonstrated its

clinical potential[10,11]. The radiography was performed with pencil scanning by delivering a set of beamlets uniformly spaced. An integral depth dose (IDD) profile was measured for each spot by the detector placed as close as possible to the exit side of the patient. Because the shape of the IDDs are impacted by the transit of protons through lateral inhomogeneties in a process called range mixing, one can not directly determine the integrated relative proton stopping power, also referred to as water equivalent thickness (WET), from the measurements.

Two approaches currently exist to estimate the WET based on proton radiography data acquired with a MLIC. On the one hand, Farace *et al.*[11] implemented the idea proposed by Mumot *et al.*[12] of performing a comparison between the IDDs measured by the MLIC with those simulated by a treatment planning system. On the other hand, Krah *et al.*[13] proposed to decompose each IDD into a set of pristine Bragg curves from which the WET would be directly obtained. To spatially distribute the WET determined by the decomposition, the use of a WET map estimated from the planning CT was shown to greatly improve the results of a demosaicing step based on the radiography data only.

However, one can be concerned by the robustness of such a two-step method. In proton therapy, pencil beams exhibit a bi-dimensional Gaussian cross sectional profile. The WET estimation problem is consequently particularly ill-posed and the solution might be strongly affected by measurement noise. Moreover, the use of the planning CT in the two methods makes them sensitive to errors in the relative proton stopping power (RSP) computation and to residual set-up errors. The WET map estimate could also be altered by changes in the anatomy of the patient and relative displacements of moving organs that could take place between the CT acquisition and the proton radiography.

In this paper, we build an iterative algorithm to perform a deconvolution of the IDDs and to increase the spatial resolution of the WET map, under a sparsity asumption. Used without relying on any prior knowledge derived from the planning CT the method already outperforms in terms of accuracy the published technique mentioned above. We then propose a variant which uses the prior information of the planning CT in a robust fashion to further improve the deconvolution result and reach submillimeter accuracy. The two methods are applied to both synthetic data and actual proton radiography acquisitions on phantoms.

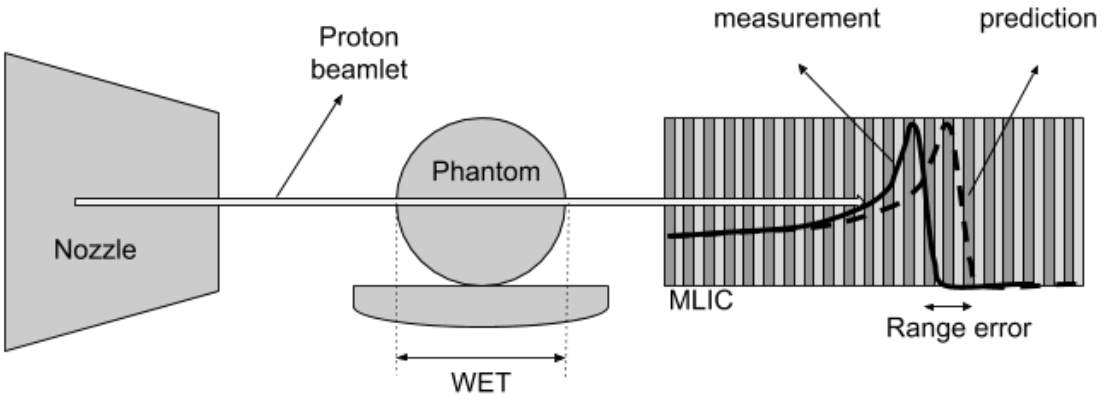

Figure 1: Schematic of a proton imager relying on a MLIC. Proton radiography can be used for quality assessment of CT conversion by computing the error between the range of the protons predicted by the treatment planning system and the measured one.

II. MATERIALS AND METHODS

Proton radiography using a MLIC does not directly provide a 2D image. As shown in Fig. 1, each pixel is not a scalar value but a sampled measurement of the proton integral depth dose (IDD) profile. A proton radiograph thus consists of a collection of IDDs from which we wish to infer the residual range or equivalently the WET of the imaged object. Eventually, the goal is to compare estimated WET values, called W_{PR}, with those predicted by the TPS, named W_{CT}. In other words, we want to determine:

$$\Delta W^{PR}(x,y) = W_{CT}(x,y) - W_{PR}(x,y) \tag{1}$$

A. Model

As experimentally demonstrated by Farace *et al.*[14] the measured IDDs, named IDD_m consist of a convolution of a Gaussian kernel G having a standard deviation equal to the spot size with shifted versions of a pristine Bragg curve called IDD_{ref} which corresponds

to the IDD that would be measured without the phantom through the beam path:

$$IDD_m(x,y,z) \approx \sum_{(x',y')\in S} G(x-x',y-y') \; IDD_{ref}(z+W(x',y')) \tag{2}$$

where (x,y) are the coordinates of each pencil beam, z refers to the depth axis of the IDD, W refers to the water equivalent thickness of the phantom along the path of the beam and S denotes the set of the indices of the pixels lying in the cross-section of the beamlet. In the case of parallel beamlets, the WET can be estimated from the HUs of the planning CT via

$$W_{CT}(x,y) = \sum_z RSP(HU(x,y,z))s_z \tag{3}$$

where RSP is usually a piecewise linear function associating to each HU the RSP[1], and s_z is the size of a voxel along the direction of the beam.

B. Deconvolution

In a previous conference proceedings paper[15], we showed that estimating the actual WET from the proton radiography data takes the form of an optimization problem:

$$W_{PR}(x,y) = \arg\min_{W(x,y)} \sum_{(x',y')\in S} \int_0^{l_d} \left(IDD_m(x',y',z) - G(x',y') * IDD_r(z+W(x',y'))\right)^2 dz \tag{4}$$

where l_d is the depth of the detector. In practice, the integral is replaced by a summation since IDD_m is sampled along z.

Because of the possible down-sampling and the convolution with a Gaussian kernel, this problem is particularly ill-posed. To deal with this, we propose to use a regularization technique relying on a sparsity assumption.

For clarity, we now use a matrix-like formulation of the equations. Eq. 2 becomes:

$$\boldsymbol{IDD_m}(z) \approx \boldsymbol{G}\ \boldsymbol{IDD_r}(z\mathbb{1} + \boldsymbol{W}) \tag{5}$$

where $\boldsymbol{G}$ is the circulant matrix associated with the convolution kernel G and $\boldsymbol{IDD_r}$ is defined by

$$IDD_{r,i}(z) = IDD_{ref}(z) \tag{6}$$

We consider a transform $\boldsymbol{\Psi}$ such that the WET can be represented through the coefficients $\boldsymbol{\alpha}$:

$$\boldsymbol{W} = \boldsymbol{\Psi\alpha} \tag{7}$$

In this study, $\boldsymbol{\Psi}$ is the matrix associated with an inverse wavelet transform.

Under sparsity assumptions, one could recover the WET by solving the problem

$$\begin{aligned} \boldsymbol{\alpha^{opt}} &= \arg\min_{\boldsymbol{\alpha}} ||\boldsymbol{\alpha}||_0 \\ &\text{s.t.} f_1(\boldsymbol{\alpha}) \leq \epsilon \end{aligned} \tag{8}$$

where the function $f_1(\boldsymbol{\alpha})$ is the similarity measure between the measured data and the model.

$$\begin{aligned} f_1(\boldsymbol{\alpha}) = \int_0^{l_d} &||\boldsymbol{IDD_m}(z) \\ &-\boldsymbol{G}\ \boldsymbol{IDD_r}(z\mathbb{1} + \boldsymbol{\Psi\alpha})||^2\, dz \end{aligned} \tag{9}$$

and where the l_0 norm $||\boldsymbol{\alpha}||_0$ transcribes the sparsity assumption.

Relaxing Eq. 8 with a l_1 norm and assuming that f_1 is convex, the minimization problem can be solved with the proximal method, which provides an iterative algorithm[16]:

$$\boldsymbol{\alpha_{n+1}} = \text{prox}_{\gamma, f_2}\left(\boldsymbol{\alpha_n} - \gamma \nabla f_1(\boldsymbol{\alpha_n})\right) \tag{10}$$

with

$$f_2(\lambda, \boldsymbol{\alpha}) = \frac{1}{2\lambda}\, ||\boldsymbol{\alpha}||_1 \tag{11}$$

The following expression was used for ∇f_1:

$$\begin{aligned}\nabla f_1(\boldsymbol{\alpha}) = 2\boldsymbol{\Psi}^T \int_0^{l_d} (\boldsymbol{DIDD_r}(z\mathbb{1} + \boldsymbol{\Psi\alpha}) \\ \circ (\boldsymbol{G}\ (\boldsymbol{G}\ \boldsymbol{IDD_r}(z\mathbb{1} + \boldsymbol{\Psi\alpha}) \\ -\boldsymbol{IDD_m}(z)))) \, dz \end{aligned} \tag{12}$$

where $\circ$ is the Hadamard product and $\boldsymbol{DIDD_r}$ is defined as:

$$DIDD_{r,i}(z) = \frac{d}{dx} IDD_{ref}(x)\bigg|_{x=z} \tag{13}$$

and was computed by finite difference.

C. Resolution enhancement

In general, the spatial resolution of the planning CT is different from the spot spacing used to acquire the proton radiograph. This can be modeled by a downsampling operator, named $\boldsymbol{D}$. The spatial resolution can now be increased to match the one of the CT using Eq. 10 and the similarity function $f_1'(\boldsymbol{\alpha})$:

$$\begin{aligned} f_1'(\boldsymbol{\alpha}) = \int_0^{l_d} ||\boldsymbol{IDD_m}(z) \\ -\boldsymbol{DG}\ \boldsymbol{IDD_r}(z\mathbb{1} + \boldsymbol{\Psi\alpha})||^2 \, dz \end{aligned} \tag{14}$$

D. Variant using the planning CT

The above method has the advantage of not involving the CT in the determination of $\boldsymbol{W}^{PR}$. Therefore, it is robust to patient misalignment or to anatomical changes. Nevertheless, an interesting variant could be to directly estimate $\Delta\boldsymbol{W}$ without going through the computation of $\boldsymbol{W}^{PR}$, ie. to calculate

$$\Delta\boldsymbol{W}^{\boldsymbol{CT}} = \arg\min_{\Delta\boldsymbol{W}} f_2(\Delta\boldsymbol{W}) \tag{15}$$

with

$$f_2(\Delta \boldsymbol{W}) = \int_0^{l_d} ||\boldsymbol{IDD_m}(z) - \boldsymbol{D\ G\ IDD_r}(z\mathbb{1} + \boldsymbol{W_{CT}} - \Delta \boldsymbol{W})||^2 \, dz \tag{16}$$

Indeed, in the absence of large anatomical changes (which is certainly the case if the proton radiograph is acquired shortly after the CT), range uncertainty is generally considered to be around 3.5%, much of which is imputed to the conversion of the planning CT into RSPs. As mentioned earlier, the majority of conversion methods from single energy CT to RSPs rely on a piecewise linear curve. Various sources of uncertainties alters this conversion process. First, the relationship between HUs and RSPs is actually not bijective. Secondly, the relevance of the model depends on the materials used to establish the curve. Usually, tables of mean composition of human tissues are used[1]. The atomic content of patient tissues may differ however and small variations in elemental compositions and in mass densities were shown to significantly change CT numbers[17]. Since single energy CT cannot be used to obtain both information, it limits the precision to which tissues can be resolved. Consequently, this limitation is also reflected into the CT conversion. Finally, inconsistencies and approximations in the mean excitation energies may also impact the conversion[2,18,19]. Considering the nature of the contributions to the range uncertainty and their accumulated magnitude (typically less than 3.5%), the sparsity assumption is even more likely to be valid on ΔW^{CT}.

Minimization of Eq. 15 shows similar conditioning characteristics to Eq. 4. First, $\Delta \boldsymbol{W^{CT}}$ may be expressed in some basis $\boldsymbol{\Psi}$ where it benefits from a sparse representation, through its coefficients $\boldsymbol{\alpha_{CT}}$:

$$\Delta \boldsymbol{W}^{CT} = \boldsymbol{\Psi \alpha_{CT}} \tag{17}$$

Then, assuming that $\Delta \boldsymbol{W_{CT}}$ can be sparse coded, problem 15 can be reformulated as:

$$\begin{aligned} \boldsymbol{\alpha}_{\boldsymbol{CT}}^{\boldsymbol{opt}} &= \arg\min_{\boldsymbol{\alpha_{CT}}} ||\boldsymbol{\alpha_{CT}}||_0 \\ \text{s.t.} f_3(\boldsymbol{\alpha_{CT}}) &\leq \epsilon \end{aligned} \tag{18}$$

where $f_3(\boldsymbol{\alpha_{CT}})$ is defined as:

$$f_3(\boldsymbol{\alpha_{CT}}) = \int_0^{l_d} ||\boldsymbol{IDD_m}(z) - \boldsymbol{G}\,\boldsymbol{IDD_r}(z\mathbb{1} + \boldsymbol{W_{CT}} - \boldsymbol{\Psi\alpha_{CT}})||^2\, dz \tag{19}$$

This problem can be solved similarly to Eq. 9 with the proximal method (Eq. 10).

E. Experimental validation

1. Proton radiography

The experimental validation relies on an anthropomorphic head phantom model 731-HN (CIRS, USA).

Proton radiography data were acquired with the commercially available MLIC named Giraffe (IBA, Belgium), according to the acquisition method described by Farace *et al.*[11]. The MLIC was placed at the exit side of the object that was imaged. The proton radiograph was acquired in pencil beam scanning mode with a primary energy of 210 MeV and a spot size of 3 mm (one sigma). For each beamlet sent at a specified location, an IDD was measured by the Giraffe. Since this device has a restricted field of view (45 x 45 mm^2), a whole radiography required several acquisitions, between each of which the object was translated. The translations were performed by moving the couch with a distance equal to the field of view. A single direction of acquisition was considered. The gantry angle was 270°, which gave a radiograph along the lateral direction.

In addition, a single energy CT scan of the head phantom was acquired at 120 kV in a 512×512 matrix, 512×512 mm^2 field of view and with a slice thickness of 1.5 mm.

2. Monte Carlo simulations

To test the WET estimation methods, we must have a set of proton radiographs for which the WET maps are accurately known. To do so, we decided to use simulations based on a x-ray CT of the object under consideration. The MLIC was modeled by a water tank added to the CT, at the exit side of the patient. Proton radiographs were simulated with the

Monte-Carlo simulation tool named MCsquare[20]. The dose maps were exported separately for each beamlet so that the IDDs could have been later reconstructed.

In order to mimic an acquisition with the Giraffe and in particular to take into account its limited field of view, a treatment plan with a specific isocenter was made for each position at which the object was placed. The IDDs obtained from those simulations were then re-sampled to correspond to the depth resolution of the Giraffe.

As for the actual measurements, the primary energy was 210 MeV and the spot size was 3 mm (one sigma). Five different spot sizes were considered: 4 mm, 5 mm, 6 mm, 7 mm and 8 mm.

To compute W, the CT was converted into RSP using the same conversion tables that were fed into MCsquare. Specifically, two tables were used by the simulation tool: one to map the HUs of the CT to mass densities and one to map the HUs to material compositions. The WET map corresponding to the simulation was then obtained by integrating the RSPs along the path of the beamlets.

3. Range uncertainty model

W_{CT} was computed with a calibration curve derived from the conversion tables used for the computation of W. To introduce differences between W_{CT} and W, random variations can be added into the calibration curve[13,21]. This was done to have a mean absolute relative error between 3% and 4%. For each spot spacing considered in this study, the deconvolution method was applied to ten different W_{CT}, each obtained with a randomly altered version of the calibration curve.

III. RESULTS

A. Deconvolution accuracy

Fig. 2 shows examples of WET maps obtained with our methods, for a spot spacing of 5 mm, a value often used for integrated-mode proton imaging[10,11,13,21]. For the method combining the planning CT, only one result among the ten performed experiments is illustrated. A WET map obtained from a range map estimated after a bi-cubic interpolation of the IDDs is also shown to provide a naive reference. It is hardly possible to visually distinguish

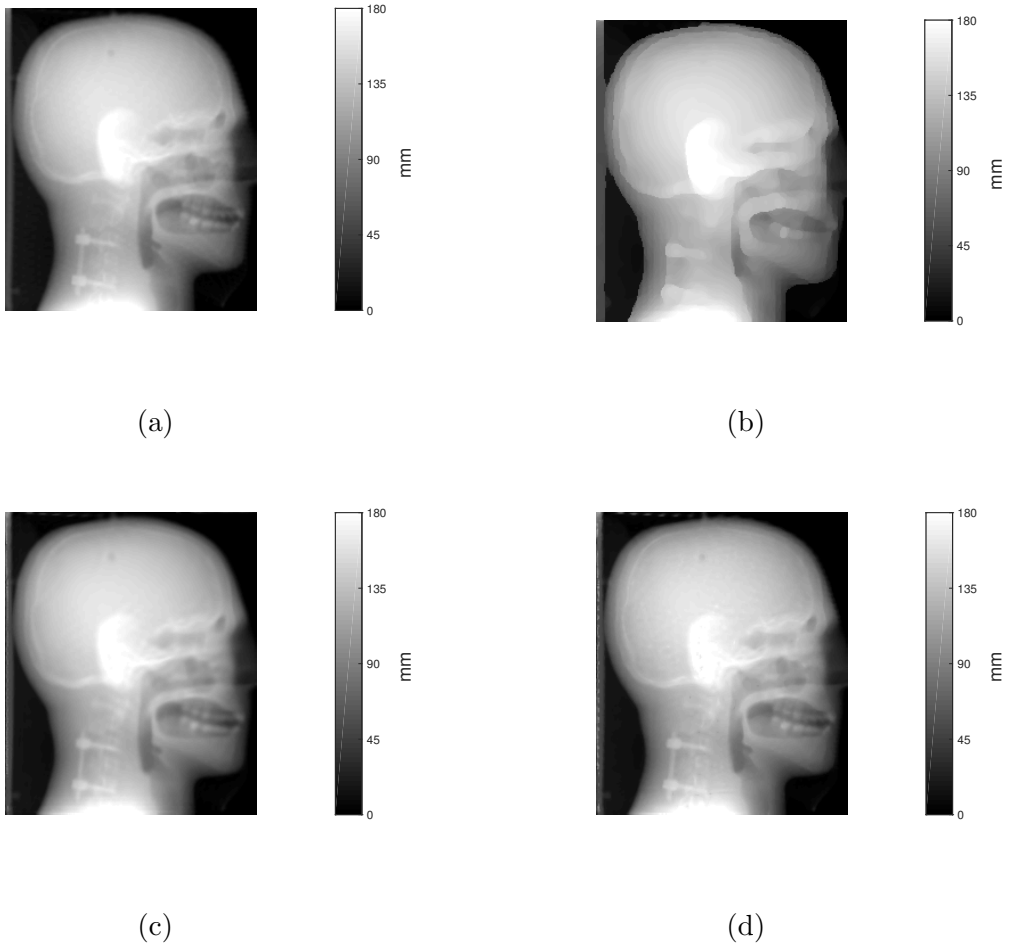

Figure 2: (a) Ground truth WET, W. (b) WET map obtained after converting a range map estimated from a bi-cubic interpolation of the IDDs (c) WET map determined through sparse deconvolution using the proton radiography data solely (d) WET map determined through sparse deconvolution with an estimate W_{CT} obtained using the planning CT.

between the ground truth data and the WET resulting from the sparse optimizations.

The difference between the optimized maps shown in Fig. 2 and the ground truth data are depicted in Fig. 3. Gamma index maps[22] are also presented for the sake of comparison with the state of the art method. The acceptance level was a relative WET difference (RWET) of 2 % and a distance to agreement (DTA) of 2 mm. The passing ratio for those values was 100 % for the two method presented in this paper and for all the considered W_{CT}. On the contrary, in a similar experiment presented in the paper of Krah *et al.*[13] with a spot spacing of 1 mm, the gamma passing rates approaches 100% only for the WET map optimized using the planning CT whereas the so-called non-optimized WET map shows large discrepancies

Method \Spacing (mm)	4	5	6	7	8
Proton radiograph only	2.7	2.3	2.8	3.8	4.3
Proton radiograph + CT	0.7	0.7	0.4	1.8	2.6

Table I: Deconvolution accuracy (95% intervals) expressed in water equivalent mm, with respect to spot spacing.

in structured phantom regions and along edges.

Fig. 4 shows the accuracy of the two optimization methods with respect to spot spacing. For the method combining the proton radiograph and the CT, the results of all the ten random experiments were aggregated for each spot spacing. The errors appeared to be almost non biased since they are symmetrically distributed around null medians.

95% intervals are listed in Table I. The accuracy is submillimeter for the second method and a spacing up to 6 mm. For the first method, the accuracy was better than 3 mm for spacings up to 6 mm.

The proposed method was also applied to real measurements as shown in Fig. 5. In Fig. 5a-b, the WET maps obtained from the acquired proton radiograph were compared with the one estimated by our treatment planning system. First, the error on the skull, at the interface with the air, seems to suggest that there remained a residual misalignement between the CT and the acquired proton radiograph, despite an accurate kV-kV alignment manually performed before the radiography. The application in post-processing of the registration method proposed by Deffet *et al.*[21] significantly decreased this error, as can be seen in Fig. 5c-d. Unfortunately, the absence of any ground truth makes it impossible to judge quantitatively the accuracy of the method on the basis of such experimental data. Nonetheless, the high resolution WET error map clearly shows that the RSP of the titanium implant was wrongly estimated, which is a striking example of the potential benefit of proton radiography since the CT conversion curve could accordingly be corrected.

IV. DISCUSSION

Range uncertainty in proton therapy is a crucial issue for which experimental data are still remarkably lacking. Among the various methods currently being investigated for *in vivo* range verification, proton radiography using a MLIC is certainly one of the easiest to implement, which is undoubtedly an advantage from the clinical point of view. Nevertheless, as

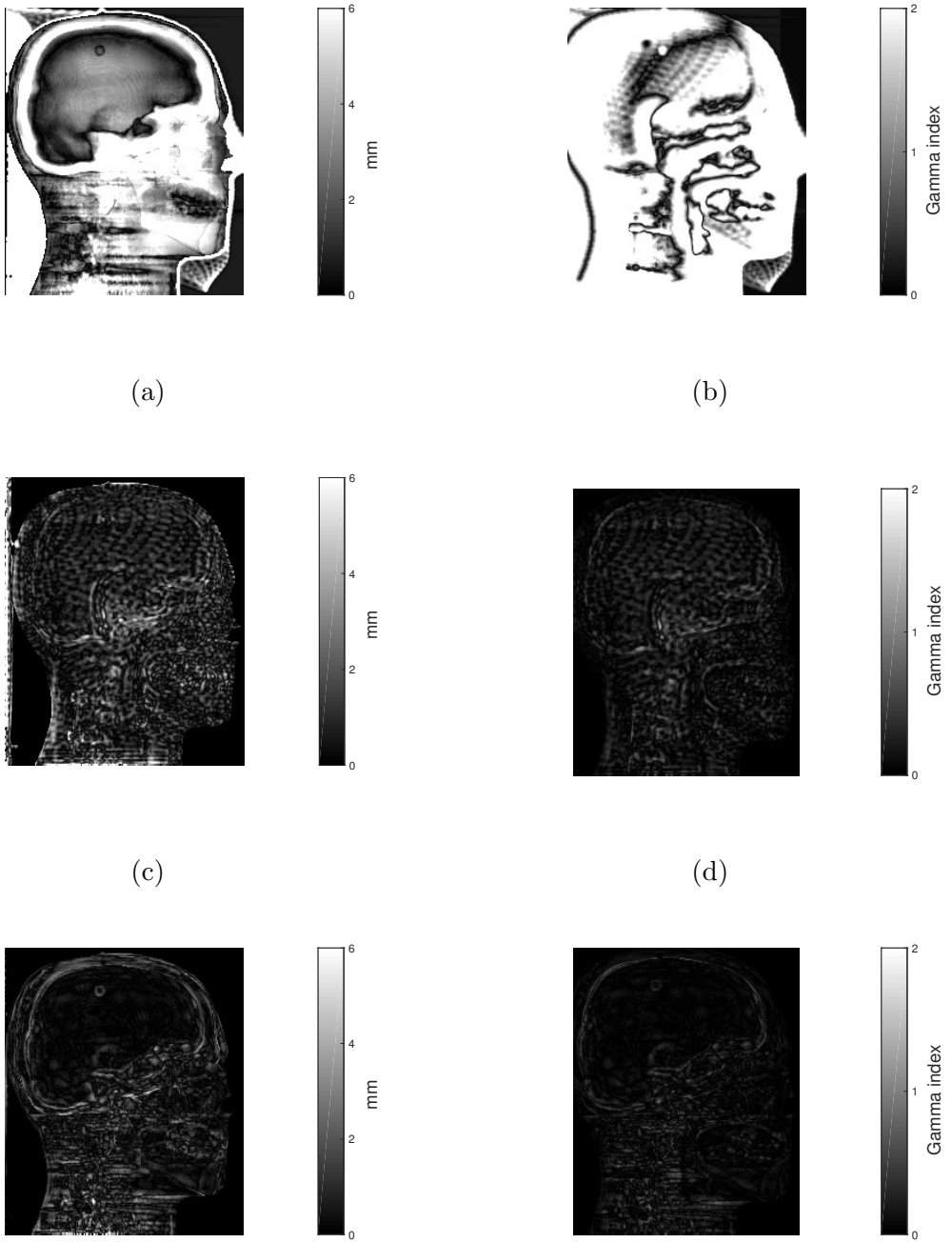

(a) (b)

(c) (d)

(e) (f)

Figure 3: Examples of (a) $|W - W_{CT}|$ (b) gamma index between W_{CT} and W (c) $|\Delta W^{PR}| = |W - W_{PR}|$ (d) gamma index between W_{PR} and W (e) $|\Delta W^{CT}|$ (f) gamma index between $W_{PR}^{CT} = W_{CT} - \Delta W^{CT}$ and W.

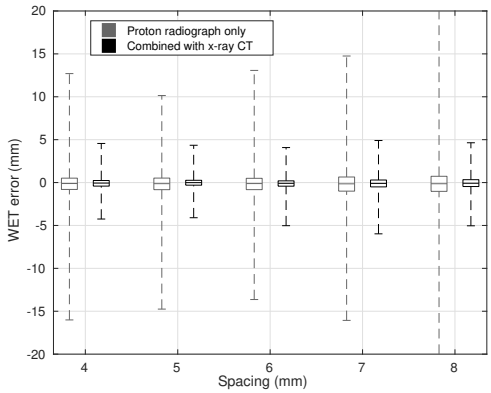

Figure 4: Deconvolution accuracy (absolute errors) expressed in water equivalent mm, with respect to spot spacing. Boxes and whiskers plot quartiles.

a technique relying on dose integration, it provides data affected by some kind of blur that were known to limit its accuracy. This is mainly a consequence of the range mixing effect induced by the interaction of proton beamlets of finite width with lateral inhomogeneities.

In addition, it is important to maintain the lowest possible imaging dose and irradiation time. To this end, it is interesting to consider the use of a larger spot spacing and mathematical methods to extract a high-range error map from this low resolution data.

The method for deblurring and increasing the spatial resolution of this type of proton radiography data explored up to this day was relying on a linear decomposition of the depth-dose profiles[13]. This problem is particularly ill-posed and obviously requires some regularization to be solved. Instead, their authors proposed the linear decomposition to be followed by a demosaicing step which uses the prior information from the planning CT. This only partially copes with the non-unicity of the linear decomposition and may potentially introduce errors caused by residual misalignment between CT and proton radiography or non-bijectivity in the relationship between HUs and RSPs.

In this paper, we presented an novel method to estimate the range error much more robustly. The sparse deconvolution of the IDDs does not make use of the conversion of the HUs into RSPs other than in the definition of the cost function. Since the planning CT is only involved in the calculation of this term, the optimization method is also less affected by residual set-up errors. Nevertheless, to study only the contribution to the range error of the HUs to RSPs conversion, it is necessary to eliminate any residual set-up error existing between the planning CT and the proton radiograph. This could be done by conventional

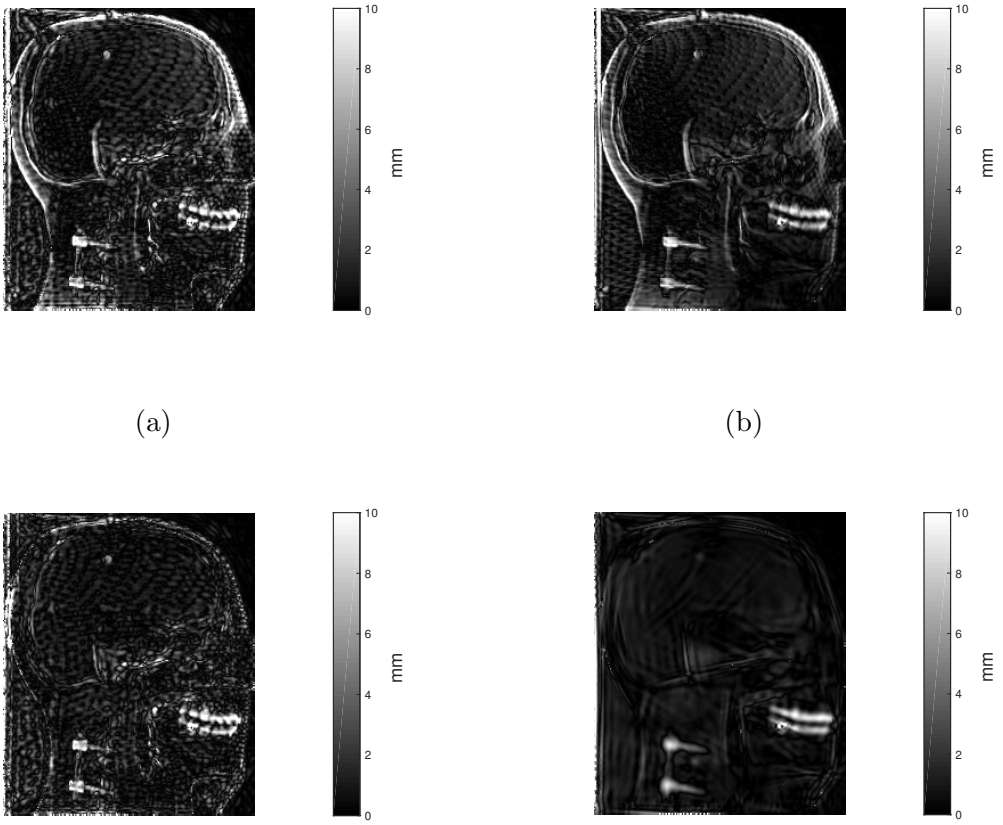

Figure 5: Absolute error maps between WET estimated from actual measurements and WET estimated based on a x-ray CT (a) from deconvolution using the proton radiograph solely (b) from deconvolution combining the proton radiograph and the x-ray CT (c) same as (a) after co-registration (d) same as (b) after co-registration.

registration methods based on a WET map estimated after the deconvolution. Nevertheless, the registration algorithm for proton radiography data proposed by Deffet et al.[15] has demonstrated a superior accuracy and can be executed prior to the deconvolution, which probably makes it possible to better condition the optimization problem by reducing the importance of the range errors to estimate.

The evaluation of the performance of the proposed iterative method was carried out on a anthropomorphic head phantom. This anatomical site is particularly well suited for proton radiography since its limited WET whatever the acquisition direction does only require moderate energy.

Monte Carlo simulations were first carried out since they are based on known WET data which provide a ground truth against which the results could be compared. For this phantom, the WET could be determined with less than 3 mm uncertainty (95% interval) using the proton radiography data only and a spot spacing smaller or equal to 6 mm. In a combination with the CT, the WET could be estimated with a submillimeter accuracy for spot spacing up to 6 mm. The error appeared to be non-biased. This is a key result in the context of CT conversion assessment where errors in the calibration curve generate systematic errors in the range estimation which are usually considered to be around 3.5% of the nominal range. The largest discrepancies were located in area presenting a high level of lateral inhomogeneities. It would however not be appropriate to consider those areas when assessing range uncertainty because of the dependence of their WET to even tiny misalignment or changes in the anatomy.

The experimental study was carried out on a perfectly rigid object. As a result, there could not be any anatomical differences between the CT and the proton radiograph. In practice and depending on the intention behind the proton radiography acquisition, there could be significant deformations that would make the deconvolution method combining CT and radiography less effective. In such a case, the accuracy would probably lie between those of the two variants presented. Ultimately, if the anatomy no longer corresponds to that of the CT, we would end up in a case where the CT does not provide any useful information and where the accuracy would probably be identical to that in the case where it is not used at all.

Finally, in addition to providing an accurate estimate of range error, an advantage of the presented method is its ability to provide a map characterized by high spatial resolution from a low resolution proton radiography which contributes to reducing the imaging dose. In the case of the head studied in this paper, we showed that it was possible to use a spot spacing up to 6 mm to estimate a range error map with pixels of size 1×1mm, hence decreasing the dose by a factor of 36.

V. CONCLUSIONS

In this paper, we have developed an algorithm to estimate range error maps from integrated-mode proton radiography data. It was tested with Monte Carlo simulations and

measurements performed with the Giraffe. WET maps with pixels of 1×1mm were estimated from proton radiographs acquired with spot spacings ranging from 4 mm to 8 mm. The larger spot spacing that could be used while maintaining submillimeter accuracy was 6 mm, thus decreasing the delivered dose by 36.

Such a WET-map could be used to assess the RSP computation in a comparison with the one that could be computed by the treatment planning system. Our experimental validation showed that this kind of comparison can be impacted by residual set-up errors which were correctly mitigated by applying the registration method for proton radiography data proposed by Deffet *et al.*[21].

CONFLICT OF INTEREST DISCLOSURE

Sylvain Deffet reports financial funding of his research by IBA (Ion Beam Applications SA, Belgium) during the confines of the study and outside the submitted work. The authors report nonfinancial support from IBA for the confines of the study.

REFERENCES

[1]U. Schneider, E. Pedroni, and A. Lomax, The calibration of CT Hounsfield units for radiotherapy treatment planning, Physics in Medicine and Biology **41**, 111 (1996).

[2]H. Paganetti, Range uncertainties in proton therapy and the role of Monte Carlo simulations, Physics in Medicine and Biology **57**, R99 (2012).

[3]A.-C. Knopf and A. Lomax, In vivo proton range verification: a review, Physics in Medicine and Biology **58**, R131 (2013).

[4]P. J. Doolan, M. Testa, G. Sharp, E. H. Bentefour, G. Royle, and H.-M. Lu, Patient-specific stopping power calibration for proton therapy planning based on single-detector proton radiography, Physics in Medicine and Biology **60**, 1901 (2015).

[5]C.-A. Collins-Fekete, S. Brousmiche, D. C. Hansen, L. Beaulieu, and J. Seco, Pre-treatment patient-specific stopping power by combining list-mode proton radiography and x-ray CT, Physics in Medicine and Biology **62**, 6836 (2017).

[6]J. Albert, R. Labarbe, and E. Sterpin, A method to optimize patient specific HU-SP calibration curve from proton range measurements, arXiv preprint arXiv:1809.01858 (2018).

[7]S. Deffet, *Proton radiography to reduce range uncertainty in proton therapy*, Université catholique de Louvain, 2018.

[8]N. Krah, V. Patera, S. Rit, A. Schiavi, and I. Rinaldi, Regularised patient-specific stopping power calibration for proton therapy planning based on proton radiographic images, Physics in Medicine & Biology **64**, 065008 (2019).

[9]R. P. Johnson, Review of medical radiography and tomography with proton beams, Reports on Progress in Physics **81**, 016701 (2018).

[10]I. Rinaldi, S. Brons, O. Jäkel, B. Voss, and K. Parodi, Experimental investigations on carbon ion scanning radiography using a range telescope, Physics in Medicine and Biology **59**, 3041 (2014).

[11]P. Farace, R. Righetto, and A. Meijers, Pencil beam proton radiography using a multilayer ionization chamber, Physics in Medicine and Biology **61**, 4078 (2016).

[12]M. Mumot, C. Algranati, M. Hartmann, J. M. Schippers, E. Hug, and A. J. Lomax, Proton range verification using a range probe: definition of concept and initial analysis, Physics in Medicine and Biology **55**, 4771 (2010).

[13]N. Krah, M. Testa, S. Brons, O. Jäkel, K. Parodi, B. Voss, and I. Rinaldi, An advanced image processing method to improve the spatial resolution of ion radiographies, Physics in Medicine and Biology **60**, 8525 (2015).

[14]P. Farace, R. Righetto, S. Deffet, A. Meijers, and F. Vander Stappen, Technical Note: A direct ray-tracing method to compute integral depth dose in pencil beam proton radiography with a multilayer ionization chamber, Medical Physics **43**, 6405–6412 (2016).

[15]S. Deffet, B. Macq, F. Vander Stappen, and P. Farace, Water Equivalent Thickness Estimation Via Sparse Deconvolution of Proton Radiography Data, in *2018 IEEE International Conference on Acoustics, Speech and Signal Processing (ICASSP)*, pages 781–785, 2018.

[16]P. Combettes and V. Wajs, Signal Recovery by Proximal Forward-Backward Splitting, Multiscale Modeling & Simulation **4**, 1168–1200 (2005).

[17]M. Yang, G. Virshup, J. Clayton, X. R. Zhu, R. Mohan, and L. Dong, Theoretical variance analysis of single- and dual-energy computed tomography methods for calculating proton stopping power ratios of biological tissues, Physics in Medicine and Biology **55**, 1343 (2010).

[18]P. Andreo, On the clinical spatial resolution achievable with protons and heavier charged particle radiotherapy beams, Physics in Medicine and Biology **54**, N205 (2009).

[19]V. De Smet, R. Labarbe, F. Vander Stappen, B. Macq, and E. Sterpin, Reassessment of stopping power ratio uncertainties caused by mean excitation energies using a water-based formalism, Medical Physics **45**, 3361–3370 (2018).

[20]K. Souris, J. A. Lee, and E. Sterpin, Fast multipurpose Monte Carlo simulation for proton therapy using multi- and many-core CPU architectures, Medical Physics **43**, 1700–1712 (2016).

[21]S. Deffet, B. Macq, R. Righetto, F. Vander Stappen, and P. Farace, Registration of pencil beam proton radiography data with X-ray CT, Medical Physics **44**, 5393–5401 (2017).

[22]D. A. Low, W. B. Harms, S. Mutic, and J. A. Purdy, A technique for the quantitative evaluation of dose distributions, Medical Physics **25**, 656–661 (1998).